Cover Page

Universiteit Leiden

The handle http://hdl.handle.net/1887/22212 holds various files of this Leiden University dissertation.

Author: Wilde, Adriaan Hugo de
Title: Host factors in nidovirus replication
Issue Date: 2013-11-13

Chapter 5

A kinome-wide siRNA screen identifies proviral and antiviral host factors in SARS-coronavirus replication, including PKR and early secretory pathway proteins

Adriaan H. de Wilde[†], Kazimier F. Wannee[†], Florine E.M. Scholte, Jelle J. Goeman, Peter ten Dijke, Eric J. Snijder, Marjolein Kikkert[‡], and Martijn J. van Hemert[‡]

[†,‡] These authors contributed equally

Manuscript submitted

ABSTRACT

To identify host factors that influence SARS-coronavirus (SARS-CoV) replication, we performed an siRNA library screen targeting the human kinome. Protein kinases are key regulators of many cellular functions and the systematic knockdown of their expression should provide a broad perspective on factors and pathways promoting or antagonizing coronavirus replication. In addition to 40 proviral proteins that promote SARS-CoV replication, our study identified 90 factors with an antiviral effect. Pathway analysis grouped subsets of these factors in specific cellular pathways, like the innate immune response and the metabolism of complex lipids, which thus appear to play an important role in SARS-CoV-infected cells. Two factors were selected for more extensive validation and follow-up experiments. In cells depleted for the beta 2 subunit of the coatomer protein complex (COPB2), the strongest proviral hit, we observed reduced SARS-CoV protein expression and a 2-log reduction in virus yield. The effect of knockdown of the COPB2-related factors COPB1 and Golgi-specific brefeldin A-resistance guanine nucleotide exchange factor 1 (GBF1) also suggested that COPI-coated vesicles and/or the early secretory pathway are important for SARS-CoV replication. Depletion of the antiviral double-stranded RNA-activated protein kinase (PKR) enhanced virus replication, and validation experiments using PKR-directed siRNAs confirmed increased SARS-CoV protein expression and virus production upon PKR depletion. The inventory of pro- and antiviral host factors and pathways described in this study expands our understanding of the replication of SARS-CoV, and may contribute to the identification of novel targets for antiviral therapy.

INTRODUCTION

Positive-stranded RNA (+RNA) viruses interact with the infected host cell at many levels during their replicative cycle, and thus far numerous host cell proteins with a role in virus replication have been identified [60-65]. These include on the one hand host factors that are used by the virus during the various stages of its life cycle, and on the other hand factors that are part of the host defense against virus infection. Such proteins may constitute interesting targets in the development of novel antiviral strategies, as drug resistance is less likely to develop when cellular rather than viral functions are targeted. Antiviral drug resistance is a serious problem, in particular when combating RNA viruses, due to their high mutation rate and potential for rapid adaptation.

Systems biology approaches have been instrumental in advancing our knowledge of individual proteins and cellular pathways that influence +RNA virus infection. For example, systematic functional genomics screens using small interfering RNA (siRNA) libraries have identified numerous host genes with a role in the replication of important human pathogens like West Nile virus [334], Dengue virus [335], human immunodeficiency virus 1 [336], hepatitis C virus [337-342], and influenza virus [338, 343, 344]. For coronaviruses a number of relevant host proteins were previously described ([321], and reviewed in [65, 320]), but the use of larger-scale siRNA screens to systematically identify such factors was not documented thus far.

Coronaviruses, and other members of the order Nidovirales [286], have the largest RNA genomes known to date (27-31 kb [37]) and the complexity of their molecular biology clearly distinguishes them from other +RNA virus groups. Although infection with most human coronaviruses is associated with relatively mild respiratory disease [19, 345], the 2003 outbreak of severe acute respiratory syndrome (SARS) highlighted the potential of coronaviruses to cause lethal disease in humans. The zoonotic transfer of SARS-coronavirus (SARS-CoV), which likely originated from bats, initiated an outbreak that affected about 8,000 humans, with a mortality of about 10% [317]. Strikingly, a similar outbreak of coronavirus-induced severe respiratory disease has been developing in a number of Arab countries since April 2012, with 9 of the 15 confirmed cases thus far (March 2013) having a fatal outcome (http://www.who.int/csr/don/archive/disease/coronavirus_infections/en/). The causative agent, human coronavirus EMC/2012, was recently identified as a previously unknown member of betacoronavirus subgroup 2c [15, 16]. Although the source of this emerging human pathogen remains to be identified, it is striking that – as in the case of SARS-CoV - its closest known relatives are coronaviruses circulating in bats [16]. These recent developments highlight once again the relevance of the systematic dissection of coronavirus-host interactions and the development of antiviral approaches to combat coronavirus infection.

Many aspects of coronavirus molecular biology remain poorly understood. SARS-CoV RNA synthesis, like that of many +RNA viruses [56], takes place at modified cytoplasmic membranes [30, 53]. The viral replication and transcription complexes (RTCs) are associated with a reticulovesicular network (RVN) of modified endoplasmic reticulum [30], which is thought to form a suitable microenvironment for RNA synthesis and possibly protects against cellular antiviral activities. Multiple host factors and cellular processes are likely involved in RVN formation and also the RTCs themselves may include various host factors in addition to the SARS-CoV nonstructural proteins (nsps) that drive viral RNA synthesis.

Previous studies identified a number of interactions between coronavirus factors and the antiviral immune response [65, 277, 320, 321]. Several evasion mechanisms were attributed to protein functions that can be either conserved across CoVs or specific for certain CoV lineages. Proteins such as nsp1 [346], the nsp3 papain-like proteinase [347], the nsp16 2′-O-methyltransferase [348], the nucleocapsid (N) protein [349], and the products of SARS-CoV ORFs 3b, 6, and 7a [105, 109, 350, 351] have all been reported to prevent interferon (IFN) induction and/or signalling.

To gain more insight into the role of host factors in the replicative cycle of SARS-CoV, we set out to systematically identify kinase-regulated cellular processes that influence virus replication. Protein kinases are key regulators in signal transduction and control a wide variety of cellular processes. Thus, assessing their relevance for virus replication can provide a broad perspective on cellular factors and pathways that influence SARS-CoV replication, as previously illustrated by studies identifying cellular kinases as host factors in various stages of the replicative cycle of other +RNA viruses [340, 341, 352, 353].

In this study, we screened an siRNA library that targets the cellular kinome (779 genes) and identified 40 proviral and 90 antiviral factors, whose depletion significantly reduced or enhanced SARS-CoV replication, respectively. Pathway analysis grouped several subsets of hits in specific cellular pathways, suggesting that these play an important role in the SARS-CoV-infected cell. Two prominent hits from the siRNA screen, the proviral beta 2 subunit of the coatomer complex (COPB2) and the antiviral double-stranded RNA-activated protein kinase (PKR), were selected for independent validation and follow-up analysis, which confirmed their importance for SARS-CoV replication. Our data offer a glimpse into the complex interplay between SARS-CoV and the host cell, and provide a basis for more focused studies to enhance our understanding of coronavirus replication and coronavirus-host interactions.

MATERIALS AND METHODS

Cell culture, viruses, and virus titration

293/ACE2 [74] and Vero E6 cells were cultured as described previously [354]. SARS-CoV strain Frankfurt-1 [208] and GFP-expressing recombinant SARS-CoV (Urbani strain) [324] were used to infect cell monolayers as described previously [354]. Virus titrations were performed essentially as described before [355]. All work with live wild-type (wt) SARS-CoV and SARS-CoV-GFP was performed inside biosafety cabinets in a biosafety level 3 facility at Leiden University Medical Center.

siRNA library and transfection reagents

The ON-TARGETplus SMARTpool Protein Kinases siRNA Library that targets the mRNAs of 779 genes, comprising the complete human kinome and some additional targets, was obtained from Dharmacon. Each individual siRNA SMARTpool consisted of four siRNAs targeting the same gene. A non-targeting (scrambled) siRNA (cat. nr. D-001810-10; Dharmacon) served as a negative control and a GAPDH-targeting siRNA (cat. nr. D-001830-10; Dharmacon) was used to routinely monitor transfection and knockdown efficiency. Stock solutions (2 µM) of siRNA SMARTpools were prepared by dissolving 0.5 nmol of siRNA SMARTpools in 250 µl of 1x siRNA buffer (60 mM KCl, 6 mM HEPES (pH 7.5), 0.2 mM $MgCl_2$; Dharmacon), according to the manufacturer's instructions. Using a 96-well pipettor (Rainin Liquidator 96), the contents of the siRNA library master plates were aliquoted into volumes appropriate for individual screening experiments. The resulting ten deep-well 96-well library plates (Greiner Bio-One) were stored at -80°C until further use.

siRNA library screening

In each siRNA screen, 293/ACE2 cells in 96-well plates containing ~10^4 cells per well were transfected with a 100-µl mixture containing 100 nM siRNA, 0.2 µg DharmaFECT1 (Dharmacon), OptiMEM (Invitrogen), and antibiotic-free cell culture medium, supplemented with 8% FCS and 2.5mM L-Glutamine, according to the manufacturer's instructions. Transfection mixes were prepared in the ten deep-well 96-well plates that together contained the complete library of 779 siRNA SMARTpools (see above). Using the contents of these library plates, we transfected black and transparent 96-well plates with 293/ACE2 cells, each in triplicate. For a schematic representation of the experimental set-up and plate lay-out, see Figs. 2A and 3A. Transfection of individual siRNA duplexes targeting PKR (cat. nr. LU-003527-00; Dharmacon), or siRNA SMARTpools targeting COPB1 (cat. nr. L-017940-01) and GBF1 (cat. nr. L-019783-00) was performed as described previously [354]. Twenty-four hours post transfection (p.t.), the medium was replaced, and cells were incubated for another 24 h at 37°C. At 48 h p.t., cells were infected with SARS-CoV-

GFP at an MOI of 10, and 24 h later they were fixed with 3% paraformaldehyde (PFA) in PBS. GFP expression was quantified by measuring fluorescence in a 96-well plate reader (Berthold Mithras LB 940), using excitation and emission wavelengths of 485 and 535 nm, respectively. The fluorescence in wells containing mock-infected cells was used to correct for background signal.

GAPDH and cell viability assays

At 48 h p.t., GAPDH enzyme activity in lysates of siRNA-transfected cells was measured using the KDalert™ GAPDH Assay Kit (Ambion) according to the manufacturer's instructions. Possible cytotoxic effects of siRNA transfection were analyzed (in triplicate) at 48 h p.t., using the CellTiter 96® AQ_{ueous} Non-Radioactive Cell Proliferation Assay (Promega). After 90 min, the reaction was terminated by the addition of 25 µl of 10% SDS and absorbance at 490 nm (A_{490}) was measured using a 96-well plate reader (Berthold).

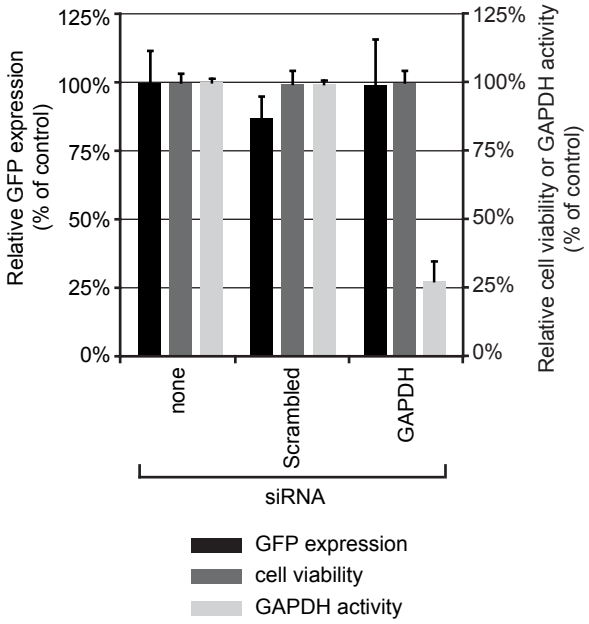

Fig. 1. siRNA-transfected 293/ACE2 cells are susceptible to SARS-CoV infection. 293/ACE2 cells were transfected with siRNAs targeting GAPDH mRNA and a scrambled control siRNA. At 48 h p.t., the cells were infected with SARS-CoV-GFP (MOI 10) and 24 h later cells were fixed and GFP fluorescence was measured (black bars). Cell viability (dark grey bars) was analyzed at 48 h after siRNA transfection and knockdown of GADPH expression was monitored by measuring enzymatic activity (light grey bars). All values were normalized to those obtained with non-transfected control cells (100%).

Data analysis

Raw data from GFP fluorescence and cell viability measurements were analyzed per individual screen with the Bioductor/R package CellHTS2 [356] with minor modifications (see results section and Fig. 2B for details). The average GFP expression (n=3) and cell viability were calculated and normalized to the signals of scrambled siRNA-transfected (control) cells. A two-sided one-sample Student's *t* test was used on the $\log_2$-transformed normalized values to determine the significance ($p < 0.05$) of the changes in GFP expression caused by siRNA transfection. The siRNA transfection was considered non-cytotoxic when the normalized cell viability assay readings (A_{490}) were above 0.85 ($p < 0.05$). Significance was determined using a one-sided one-sample Student's *t* test on the $\log_2$-transformed normalized values using $\mu \leq 0.85$ as the null hypothesis.

Gene silencing using lentivirus-expressed shRNAs

Vectors for expression of short hairpin RNAs (shRNAs) targeting human COPB2 (cat. nr. TRCN-065114; accession nr. NM_004766) or human PKR (cat. nr. TRCN-001382; accession nr. NM_002759) were picked from the MISSION TRC-1 library of shRNA-expressing lentiviruses (Sigma) and lentivirus stocks were prepared according to the manufacturer's instructions. A lentivirus expressing a non-targeting (scrambled) shRNA (cat. nr. SHC-002) was used as negative control. Lentivirus particle titers were determined using a p24 ELISA (Zeptometrix) according to the manufacturer's instructions. Wells (4 cm^2) containing 8 x 10^4 293/ACE2 cells were transduced with shRNA-expressing lentiviruses at an MOI of 3 in culture medium containing 8 µg/ml polybrene, and after 24 h fresh medium was given. At 72 h p.t., cells were infected with wt SARS-CoV or SARS-CoV-GFP (MOI 0.01), or depletion of COPB2 or PKR was validated by Western blot analysis of cell lysates using target-specific antibodies.

Protein analysis and antibodies

Total cell lysates were prepared in 4x Laemmli sample buffer (100 mM Tris-HCl, pH 6.8, 40% glycerol, 8% sodium dodecyl sulfate (SDS), 40 mM DTT, 0.04 mg/ml bromophenol blue), after which samples were heated at 95°C for 15 min. Following SDS-PAGE, proteins were transferred to Hybond-LFP membranes (GE Healthcare) by semi-dry blotting, and membranes were blocked with 1% casein in PBS containing 0.1% Tween-20 (PBST). The following antisera against cellular proteins were used: rabbit anti-PKR (cat. nr. 610764; BD Biosciences), goat anti-COPB2 (sc-13332; Santa-Cruz), and mouse monoclonal antibodies against β-actin (A5316; Sigma) and the transferrin receptor (TfR; cat. nr. 13-6890; Invitrogen). Rabbit antisera against SARS-CoV nsp8 and N protein [30, 52] were used to analyze viral protein expression. After overnight incubation with the primary antibody, membranes were probed with biotinylated secondary antibodies (biotinylated rabbit anti-goat, swine anti-rabbit, or goat anti-mouse) for 1 h at RT, after which a tertiary

mouse anti-biotin-Cy3 antibody was used to visualize protein bands using a Typhoon 9410 scanner (GE Healthcare).

Canonical pathway analysis

The Ingenuity Pathway Analysis (IPA™) package was used to place hits in canonical cellular pathways. The significance of the association between the data set and the respective pathways was determined in two ways: (i) the number of molecules from the

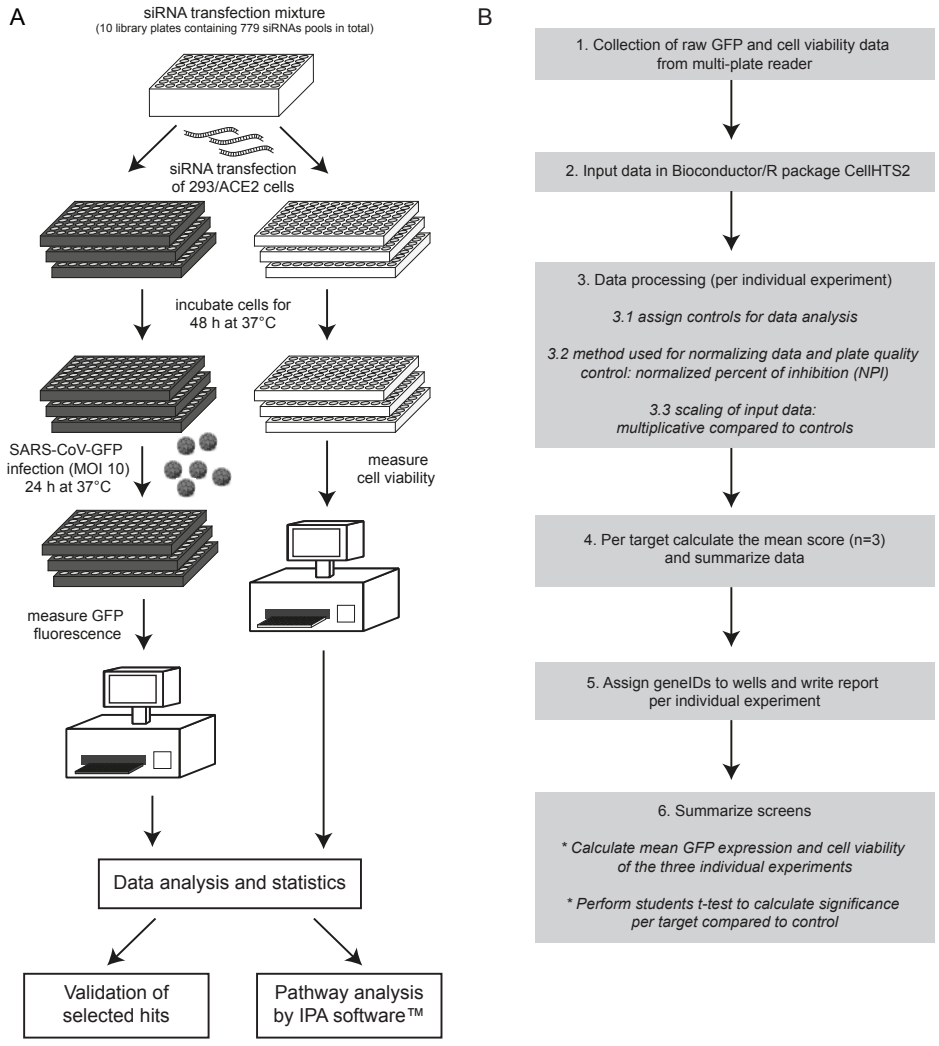

Fig 2. siRNA library screening procedure and data analysis. (A) Schematic overview of the experimental design of the siRNA library screen. See text for details. (B) Flow chart outlining the data analysis procedure that was performed with the Bioconductor/R package CellHTS2. See text for details.

data set that map to a specific pathway divided by the total number of molecules in that canonical pathway (the higher the percentage of hits identified in a specific pathway, the higher the likelyhood it plays a role in the viral replicative cycle); (ii) Fisher's exact test was used to determine the probability that the association between the genes in the dataset and the canonical pathway is explained by chance alone.

RESULTS

Developing siRNA library screening for host factors involved in nidovirus replication.

A commercial human kinome-directed siRNA library (779 targets) was used to assess the effect of systematic knockdown of individual host kinases on the replicative cycle of the coronavirus SARS-CoV (this study) and the distantly related arterivirus EAV (K. F. Wannee, A. H. de Wilde *et al*., unpublished data). We performed our siRNA screens in 293/ACE2 cells [74], which express the SARS-CoV receptor angiotensin-converting enzyme 2 and, in contrast to other cell lines tested, were found to be permissive to infection with both SARS-CoV and EAV. This property facilitates direct comparative studies between these two distantly related nidoviruses [354]. Furthermore, 293/ACE2 cells could be efficiently transfected with siRNAs, as illustrated by a consistent ~75% reduction of GAPDH activity at 48 h p.t. with an siRNA SMARTpool targeting the GAPDH mRNA (Fig. 1; light grey bars). No change in cell viability was detected by 48 h p.t. following transfection with either a scrambled siRNA or the GAPDH-specific siRNA (Fig. 1; dark grey bars). When these siRNA-transfected 293/ACE2 cells were subsequently infected with SARS-CoV-GFP (MOI 10), no significant differences in GFP expression were observed at 24 h p.i. compared to control cells that had not been transfected with siRNAs. This demonstrated that the siRNA transfection procedure per se did not adversely affect SARS-CoV-GFP replication (Fig. 1; black bars).

siRNA screening for host kinases involved in SARS-CoV replication.

A human kinome-directed siRNA screen was performed to identify host cell kinases that affect SARS-CoV-GFP replication, according to the experimental set-up outlined in Fig. 2A. For each independent siRNA screening experiment, we used a set of ten 96-well library plates, each containing approximately 80 specific siRNA SMARTpools and several controls (see plate layout in Fig. 3A). Transfection mixes (final concentration of 100 nM siRNA) were prepared in these library plates and their contents was used to transfect - per library plate - 293/ACE2 cells in three black and three transparent 96-well plates. Forty-eight hours after siRNA transfection, the black plates were infected with the SARS-CoV-GFP reporter virus (MOI 10), and at 24 h p.i. GFP expression was analyzed by

fluorimetric quantitation. At the moment of infection, the transparent plates were used to monitor (potential) cytotoxic effects of siRNA transfection using a colorimetric cell viability assay. The complete siRNA screen, i.e. the viability controls and the quantitation of SARS-CoV-driven GFP expression (in triplicate for each siRNA), was repeated three times, after which data sets were processed as outlined in Fig. 2B. The data, obtained from a 96-well plate reader (step 1) were processed with the Bioconductor/R package CellHTS2 as described [356] (step 2). Experimental controls were assigned (step 3.1 and Fig. 3A), and the NPI method (normalized percent of inhibition; step 3.2) was used to normalize GFP fluorescence values to those of scrambled siRNA-transfected cells, and to correct for plate-to-plate variation. Subsequently, the GFP data were transformed to a multiplicative scale (the value obtained using scrambled siRNA-transfected cells was set to 1; step 3.3). Next, the results for each replicate library screen were summarized and used for further data analysis (step 4), including the assignment of GeneIDs to each well (step 5). Finally, the data of the three independent library screens were combined and summarized (step 6).

The processed data output of a representative library screen, showing the distribution of the hits for each plate, is depicted in Fig. 3A. Column 1 of each plate contained the infected control cells described above, whereas column 12 contained mock-infected cells. Host cell kinases were considered to have a proviral effect when their siRNA-mediated knockdown reduced the GFP signal (negative score values) and kinases were considered antiviral when the GFP signal increased upon their knockdown (positive score values). Graphical representations of the hit distribution per plate were visually inspected in order to minimize the chance of false positive or false negative hits due to major (technical) artifacts (Fig. 3A).

Using scrambled siRNA-transfected control cells as a reference, the knockdown of most cellular kinases was found to be non-cytotoxic within the time frame of this experiment (Fig. 3B and Data set S1). The cut-off value below which siRNA treatment was considered to be toxic was set at 85% cell viability relative to scrambled siRNA-transfected control cells ($p < 0.05$) (Fig. 3B). Using this criterion, 222 out of 779 (28.5%) transfections with the specific siRNA pools appeared to be toxic to the cells. A minor fraction (50 targets; 6.4%) appeared to be highly detrimental (normalized viability value below 75%). To prevent false-positive proviral hits due to a general negative effect on cell viability or cell division, we excluded all targets whose knockdown was associated with viability measurements below 85%. Such data filtering was not applied for antiviral hits (i.e. knockdown enhancing GFP expression) since siRNA-induced cytotoxicity is expected to inhibit virus replication and should therefore not give rise to false-positive antiviral hits.

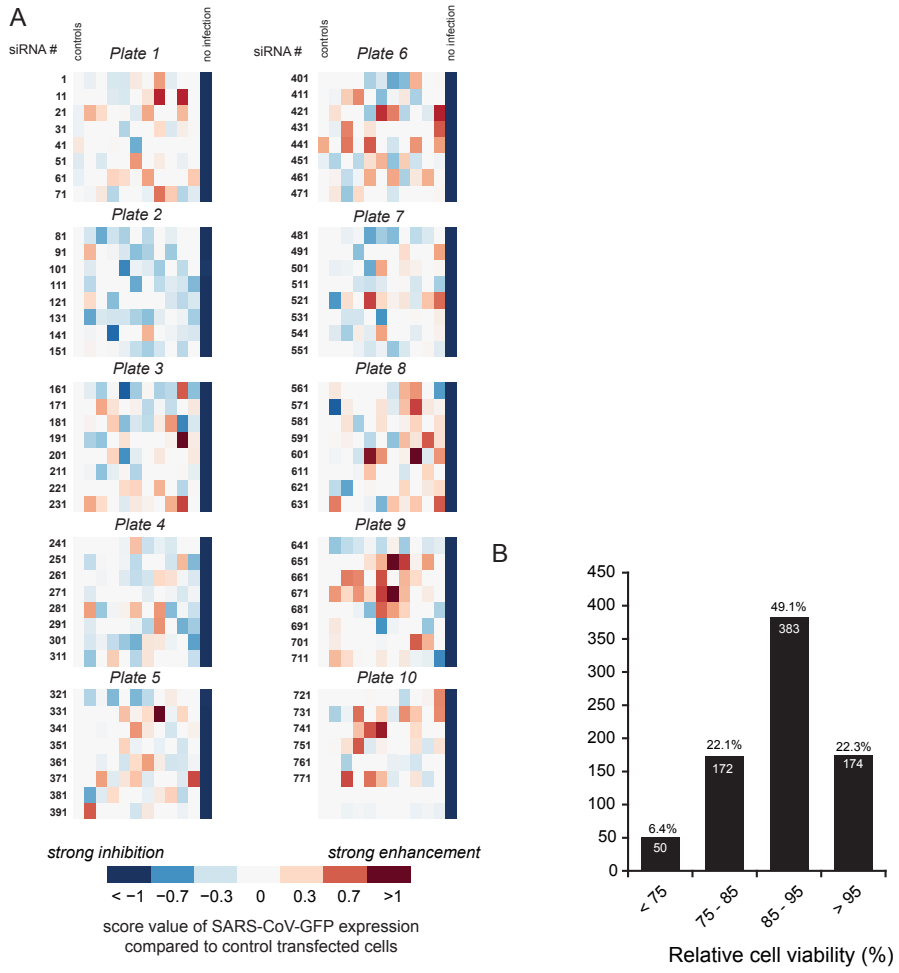

Fig. 3. Quality plots of the siRNA screen for host factors involved in SARS-CoV replication. (A) Plate-wise quality-plots of the score values for one replicate of a representative siRNA library screen. In total, three screens, each consisting of three replicates, were performed. Score values of -1, 0, and 1 represent 0%, 100%, and 200% SARS-CoV-driven GFP expression compared to infected control wells, respectively. Cells transfected with control siRNAs were present in the first column ("controls") of each plate, while the cells in column 12 were mock-infected to allow correction for background GFP signal. The remaining wells of each plate (columns 2-11) contained cells transfected with the siRNA SMARTpools. The GFP expression level in each well compared to that of control siRNA-transfected cells (score value) is represented by the color-coded squares according to the legend below panel A. (B) Relative cell viability of cells transfected with the 779 siRNA pools in the kinome-wide siRNA library. Viability assays were done at 48 h p.t. and the data were normalized to the measurements for control cells transfected with scrambled siRNA (100%). Data were binned into 4 viability categories and the number in each bar is the absolute number of targets within that category, which represents the percentage of the 779 siRNA targets in the screen that is indicated above each bar. The viability data are the average of three independent library screens, each including triplicate measurements for each siRNA pool in the library.

Identification of proviral and antiviral hits and pathways influencing SARS-CoV-GFP infection.

After exclusion of toxic siRNA SMARTpools that decreased GFP expression (see above), the remaining 684 targets were ranked on the basis of the GFP signal measured in SARS-CoV-GFP-infected cells (log_2-fold GFP expression compared to control cells; Fig. 4). Targets were qualified as antiviral or proviral hits if GFP expression differed significantly from that in control cells transfected with the scrambled siRNA pool ($p < 0.05$). Knockdown of the majority of the targets (552 proteins) did not significantly alter GFP reporter gene expression ($p > 0.05$). However, as common in this kind of screening experiments, we cannot formally exclude that our results may have been influenced by insufficient knockdown of certain target genes by the library's siRNA pools.

Using the criteria outlined above, a total of 90 cellular proteins (19.4% of all targets) were identified as antiviral factors, since their depletion significantly increased GFP expression. For 36 of these antiviral hits, knockdown resulted in an increase of at least 1.5-fold (Fig. 5A). Forty proviral factors were identified and the knockdown of nine of those reduced GFP expression by more than 2-fold (Fig. 5B; for the complete data set, see Dataset S2).

Although, according to the criteria formulated above ($p < 0.05$), ANGPT4 (214%; $p = 0.0555$) and PKR (210%; $p = 0.0884$) formally did not qualify as antiviral hits, we have included these proteins in view of the exceptionally strong stimulation of GFP expression triggered by their knockdown (Fig. 5A). Furthermore, since its knockdown resulted in an almost 3-fold decrease of GFP signal (35%; $p = 0.0004$), DGKE was included as a proviral hit, despite the fact that the viability assay did not rigorously exclude cytotoxic effects for this siRNA pool (viability 88%, $p = 0.0540$).

The pro- and antiviral hits identified in the siRNA screen were mapped to cellular pathways using the IPA software package. Fig. 6 shows the canonical pathways and more general functional categories (highlighted in color) in which the proviral (red) and antiviral (green) hits were strongly represented ($p < 0.05$). The pathways included apoptosis, cellular immune response, growth factor signaling, cellular homeostasis, metabolism of complex lipids, and intracellular and second messenger signaling.

Validation of COPB2 as a proviral factor in SARS-CoV replication.

COPB2 (or β'-COP) was identified as the strongest proviral hit in our screen, as its knockdown resulted in an 82% decrease of GFP expression ($p = 0.0143$; Fig. 5B). The coatomer protein complex, of which COPB2 is a subunit, contains a total of seven protein subunits (α-, β-, β'-, γ-, δ-, ε-, and ζ-COP), and drives the formation of COPI-coated vesicles, which function in retrograde transport in the early secretory pathway [357]. To validate its role as a proviral host factor in SARS-CoV replication, COPB2 was depleted by transducing 293/ACE2 cells with lentiviruses expressing COPB2 mRNA-specific shRNAs. This reduced

COPB2 levels by ~70%, compared to control cells transduced with a lentivirus expressing a scrambled shRNA (Fig. 7A), and this reduction in COPB2 levels did not affect cell viability (Fig. 7B). Subsequent infection of COPB2-depleted cells with SARS-CoV-GFP (MOI 0.01) resulted in a decrease of N protein and GFP expression at 32 h p.i. (Fig. 7C; left panel). To verify that knockdown experiments with recombinant SARS-CoV-GFP properly reflected the characteristics of the wt virus, we analyzed viral protein expression and

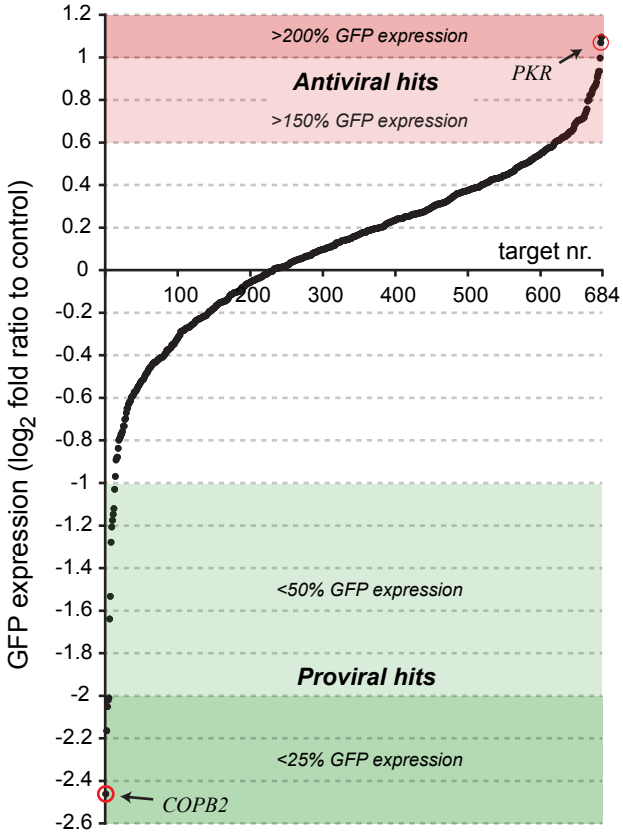

Fig. 4. Results of the siRNA screens for host factors influencing SARS-CoV replication. The plot shows the distribution of the log_2-transformed values of reporter gene expression by SARS-CoV-GFP in siRNA-transfected cells, normalized to the GFP signal of infected control cells that were transfected with scrambled siRNA. Targets were ranked based on the magnitude of the effect of their knockdown on SARS-CoV replication. Targets were considered to have an important antiviral effect when their knockdown increased reporter gene expression to at least 150% (red area above x-axis). Proviral hits, whose knockdown induced an at least 2-fold reduction in GFP expression, are depicted in the green area below the x-axis. Proviral targets whose knockdown reduced cell viability to below 85% were excluded (see main text), leaving a total of 684 targets included in the final analysis. The positions of the targets used for follow-up validation experiments (COPB2 and PKR) are indicated. The plot represents the average of three library screens (each done in triplicate).

virus yield in COPB2-depleted cells at 24 h after infection with wt SARS-CoV (MOI 0.01). As for SARS-CoV-GFP, a clear reduction in N protein expression was observed compared to cells transduced with a lentivirus expressing a scrambled shRNA (Fig. 7C; right panel). Titration of culture supernatants from SARS-CoV-GFP-infected cells (32 h p.i.) and wt SARS-CoV-infected cells (24 h p.i.) revealed a 2- to 3-log reduction for both viruses (Fig. 7D).

Proteins of the early secretory pathway are important for SARS-CoV replication.

To further substantiate the importance of COPI-coated vesicles for SARS-CoV replication, the expression of another component of the coatomer protein complex, subunit beta 1 (COPB1) was depleted by transfection of 293/ACE2 cells with a COPB1 mRNA-specific siRNA SMARTpool. After 48 h, transfected cells were infected with SARS-CoV-GFP (MOI 10) and 24 h later GFP expression was quantified. Depletion of COPB1 resulted in a reduction of SARS-CoV-driven GFP expression with 83% (Fig. 7E). The formation of COPI-coated vesicles is mediated through activation of ADP-ribosylation factor 1 (Arf1) by Golgi-specific brefeldin A-resistance guanine nucleotide exchange factor 1 (GBF1) [358]. Therefore, we also analyzed the importance of GBF1. GFP reporter gene expression by SARS-CoV-GFP was reduced by 89% in 293/ACE2 cells that had been depleted for GBF1 by siRNA transfection and were subsequently infected at 48 h p.t. (Fig. 7E). Taken together, these data suggest that COPB2 and COPI-coated vesicles play an essential role in SARS-CoV replication.

Validation of PKR as antiviral hit affecting SARS-CoV replication.

PKR was one of the strongest of the 90 antiviral hits that were identified in the siRNA library screen. In two independent follow-up experiments with PKR-specific siRNA SMARTpools, a more than 2-fold increase in GFP expression by SARS-CoV-GFP was observed (data not shown), suggesting that PKR is a bona fide antiviral hit. PKR is a serine/threonine protein kinase that is activated by double-stranded (ds)RNA, a hallmark of RNA virus infection, and the activated form of PKR blocks translation initiation through eIF-2α phosphorylation (reviewed in [68]).

To further validate the antiviral role of PKR in SARS-CoV replication, a deconvoluted set of four individual PKR-directed siRNAs was used. Transfection of 293/ACE2 cells with three of these siRNAs (numbers 2, 3, and 4) significantly increased SARS-CoV-driven GFP expression (Fig. 8A; black bars). Cell viability was slightly reduced after transfection with these PKR-directed siRNAs, in particular using siRNA 2 which caused a 14% reduction in cell viability (Fig 8A; grey bars). Nevertheless, despite the fact that this siRNA adversely affected cell viability, an increase rather than a decrease of SARS-CoV-driven GFP expression was observed.

A

GeneID	GFP expression (fold increase) 1	2	3	average	p-value	Accession	Gene name
ANGPT4	1.8	3.1	1.8	2.1	0.0555*	NM_015985	Angiopoietin 4
PKR	3.0	1.4	2.3	2.1	0.0884*	NM_002759	Double-stranded RNA-activated protein kinase
CLK1	2.1	2.1	1.8	2.0	0.0077	NM_004071	CDC-like kinase 1
MAP2K6	2.0	2.0	1.8	1.9	0.0014	NM_002758	Mitogen-activated protein kinase kinase 6
CSNK1G1	1.7	2.1	1.8	1.9	0.0067	NM_022048	Casein kinase 1, gamma 1
EPHA3	1.7	1.6	2.1	1.8	0.0176	NM_005233	EPH receptor A3
CDK6	1.7	2.1	1.7	1.8	0.0140	NM_001259	Cyclin-dependent kinase 6
AURKB	1.9	1.8	1.8	1.8	0.0016	NM_004217	Aurora kinase B
GCK	1.8	2.0	1.6	1.8	0.0119	NM_000162	Glucokinase (hexokinase 4, maturity onset diabetes of the young 2)
DGKD	1.8	1.6	2.0	1.8	0.0135	NM_003648	Diacylglycerol kinase, delta 130kDa
STK24	2.0	1.5	1.9	1.8	0.0241	NM_003576	Serine/threonine kinase 24 (STE20 homolog, yeast)
CKS1B	2.1	1.6	1.6	1.7	0.0298	NM_001826	CDC28 protein kinase regulatory subunit 1B
CLK4	1.6	2.1	1.6	1.7	0.0282	NM_020666	CDC-like kinase 4
HK1	1.6	2.1	1.5	1.7	0.0318	NM_000188	Hexokinase 1
ACVR1	1.7	1.7	1.6	1.7	0.0018	NM_001105	Activin A receptor, type I
AKAP6	1.8	1.7	1.5	1.7	0.0068	NM_004274	A kinase (PRKA) anchor protein 6
FLJ12476	1.7	1.6	1.6	1.6	0.0004	NM_022784	IQ motif containing H
LATS1	1.8	1.6	1.5	1.6	0.0074	NM_004690	LATS, large tumor suppressor, homolog 1 (Drosophila)
CDKL2	1.4	1.8	1.7	1.6	0.0265	NM_003948	Cyclin-dependent kinase-like 2 (CDC2-related kinase)
MAPK9	1.9	1.6	1.5	1.6	0.0207	NM_002752	Mitogen-activated protein kinase 9
PTPRG	1.9	1.4	1.6	1.6	0.0259	NM_002841	Protein tyrosine phosphatase, receptor type, G
BMPR2	1.7	1.4	1.8	1.6	0.0261	NM_001204	Bone morphogenetic protein receptor, type II (serine/threonine kinase)
DCK	1.6	1.5	1.7	1.6	0.0051	NM_000788	Deoxycytidine kinase
MAP2K3	1.6	1.9	1.4	1.6	0.0369	NM_002756	Mitogen-activated protein kinase kinase 3
MYO3B	1.7	1.5	1.5	1.6	0.0087	NM_138995	Myosin IIIB
EIF2AK3	1.6	1.6	1.5	1.6	0.0014	NM_004836	Eukaryotic translation initiation factor 2-alpha kinase 3
CLK3	1.7	1.6	1.4	1.6	0.0138	NM_001292	CDC-like kinase 3
FYB	1.8	1.5	1.4	1.6	0.0217	NM_001465	FYN binding protein (FYB-120/130)
ALS2CR7	1.5	1.8	1.4	1.5	0.0327	NM_139158	Cyclin-dependent kinase 15
STK25	1.7	1.4	1.6	1.5	0.0224	NM_006374	Serine/threonine kinase 25 (STE20 homolog, yeast)
HAK	1.5	1.7	1.5	1.5	0.0130	NM_052947	Alpha-kinase 2
ITK	1.6	1.5	1.5	1.5	0.0004	NM_005546	IL2-inducible T-cell kinase
MAPK1	1.6	1.5	1.5	1.5	0.0042	NM_002745	Mitogen-activated protein kinase 1
DGUOK	1.5	1.6	1.5	1.5	0.0007	NM_001929	Deoxyguanosine kinase
MVD	1.7	1.4	1.5	1.5	0.0211	NM_002461	Mevalonate (diphospho) decarboxylase
EKI1	1.7	1.4	1.4	1.5	0.0172	NM_018638	Ethanolamine kinase 1
EPHA5	1.4	1.4	1.8	1.5	0.0385	NM_004439	EPH receptor A5
DAPK3	1.4	1.7	1.5	1.5	0.0141	NM_001348	Death-associated protein kinase 3

B

GeneID	GFP expression (fold increase) 1	2	3	average	p-value	Accession	Gene name
COPB2	0.2	0.3	0.1	0.2	0.0143	NM_004766	Coatomer protein complex, subunit beta 2 (beta prime)
CDK5R2	0.2	0.4	0.2	0.2	0.0251	NM_003936	Cyclin-dependent kinase 5, regulatory subunit 2 (p39)
PFTK1	0.4	0.3	0.3	0.3	0.0087	NM_012395	PFTAIRE protein kinase 1
ABI1	0.4	0.3	0.3	0.3	0.0055	NM_005470	Abl-interactor 1
DGKE	0.3	0.4	0.4	0.4	0.0004†	NM_003647	Diacylglycerol kinase, epsilon 64kDa
NME2	0.5	0.4	0.4	0.4	0.0027	NM_002512	Non-metastatic cells 2
AZU1	0.5	0.4	0.5	0.4	0.0075	NM_001700	Azurocidin 1 (cationic antimicrobial protein 37)
IHPK1	0.5	0.3	0.5	0.5	0.0405	NM_153273	Inositol hexaphosphate kinase 1
PSKH1	0.5	0.5	0.4	0.5	0.0094	NM_006742	Protein serine kinase H1
PRKCI	0.6	0.4	0.5	0.5	0.0157	NM_002740	Protein kinase C, iota

* Note: not a significant hit (p>0.05), but PKR and ANGPT4 were also included as antiviral hits

† Note: siRNAs are slightly toxic to cells (88% viability, but p = 0.0540)

Fig. 5. Heat-maps of the identified pro- and antiviral hits. (A) List of the antiviral hits causing an at least 1.5-fold increase in GFP expression ($p < 0.05$). (B) Proviral hits yielding a more than 2-fold decrease in GFP expression ($p < 0.05$). For each target, the p-value, accession number, and gene name are shown. Each data point represents the result of a single library screen and is the average of the 3 replicates that were done in each screen.

Transfection with PKR-specific siRNAs reduced PKR levels in 293/ACE2 cells up to 87% compared to control cells, depending on the siRNA used (Fig. 8B). To verify that PKR knockdown increased wt SARS-CoV replication, siRNA-transfected 293/ACE2 cells were infected with wt SARS-CoV (MOI 0.01) and viral protein expression was analyzed at 24 h p.i. by Western blot analysis. In line with the effect of PKR siRNA 2 on 293/ACE2 cell viability (Fig. 8A), cells transfected with this siRNA contained reduced levels of β-actin, which was used as loading control (Fig. 8C; lower panel). Transfection with two of the

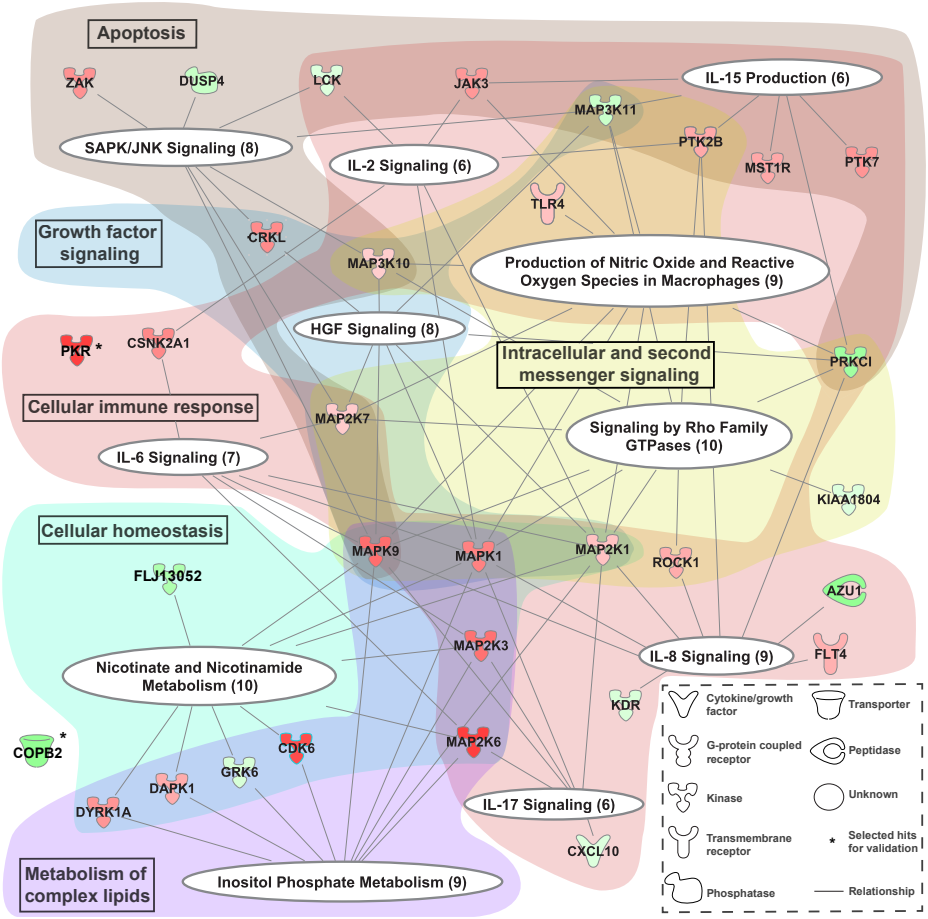

Fig. 6. Cellular pathways influencing SARS-CoV-GFP replication. Graphical representation of the canonical pathways (white ellipses) identified in the siRNA library screen for cellular factors affecting SARS-CoV replication. The proviral (red) and antiviral hits (green) are represented by nodes with lines linking them to one or more canonical pathways. The color intensity of the nodes indicates the strength of the pro- or antiviral effect (log_2 ratio of GFP expression normalized to infected control cells), e.g. factors with a stronger antiviral effect have a more intense red color. The identified canonical pathways were clustered into more general categories that are indicated by text boxes in the colored background shading.

four individual PKR-directed siRNAs (siRNA 2 and 3) clearly increased the expression of SARS-CoV N protein (Fig. 8C, upper panel), and also led to an ~1-log increase in infectious progeny titers (Fig. 8D). Taken together, the increases in GFP signal, N expression

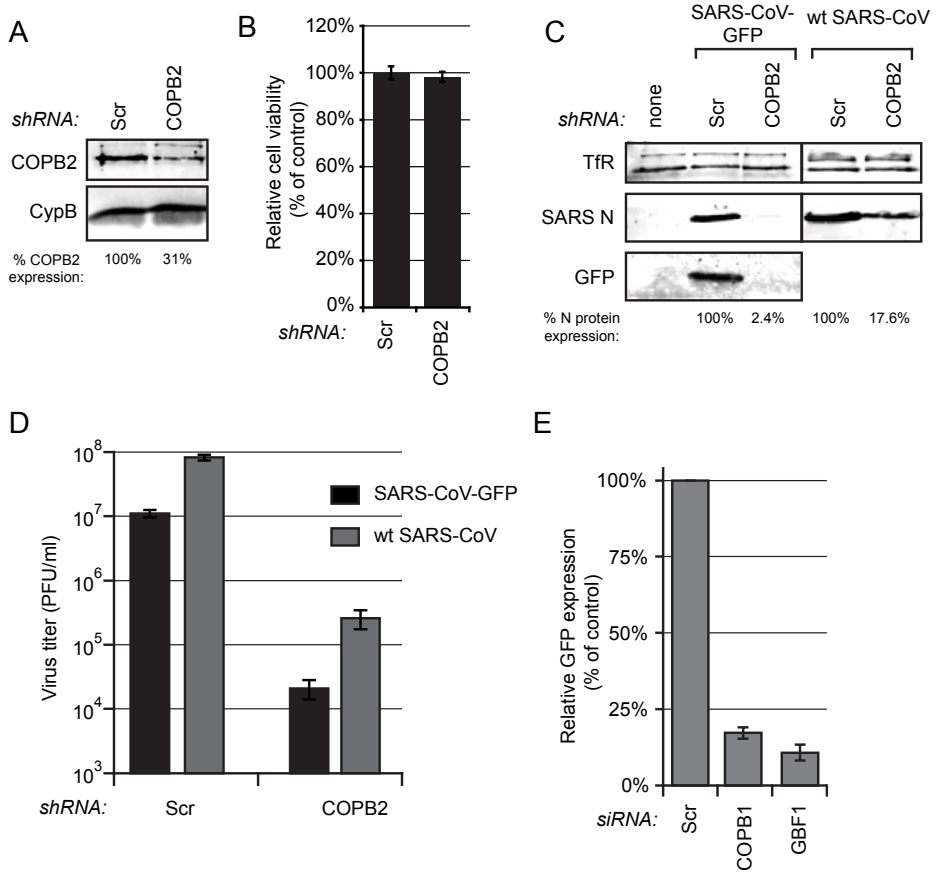

Fig. 7. Proteins of the early secretory pathway are important for SARS-CoV replication. (A) 293/ACE2 cells were transduced with lentiviruses expressing a COPB2 mRNA-specific or a scrambled shRNA. Knockdown of COPB2 expression at 48 h p.t. was monitored by Western blotting with a COPB2-specific antiserum and cyclophilin B (CypB) was used as loading control. (B) Cell viability in COPB2-depleted 293/ACE2 cells was analyzed at 48 h after transduction (% of value for cells transduced with lentiviruses expressing a scrambled shRNA). (C) COPB2-depleted and control cells were infected with either SARS-CoV-GFP or wt SARS-CoV and protein expression was analyzed by Western blotting with N-specific and GFP-specific antisera, using the TfR as a loading control. SARS-CoV N protein expression was quantified and its level normalized to the value for scrambled siRNA-transfected cells (100%) is indicated under each lane. (D) SARS-CoV-GFP (black bars) and wt SARS-CoV (grey bars) progeny titers in the culture supernatant of infected, COPB2-depleted and control cells. (E) Normalized GFP expression by SARS-CoV-GFP in 293/ACE2 cells transfected with siRNA SMARTpools targeting COPB1 or GBF1 and a scrambled control siRNA. Cells were infected 48 h p.t. at an MOI of 10 and 24 h later GFP fluorescence was quantified and normalized to that in infected cells transfected with a scrambled siRNA.

and infectious progeny titer correlate well with the magnitude of PKR knockdown, which makes an off-target effect in the initial siRNA library screen unlikely and suggests a true antiviral role for PKR in SARS-CoV infected cells.

DISCUSSION

In the past decade functional genomics studies have - in an systematic way - identified host factors that can influence the replication of diverse +RNA viruses [334, 335, 338-340, 352, 359]. We here describe a human kinome-wide siRNA screen for factors influencing the entry and replication of SARS-CoV, to our knowledge the first systematic functional genomics study of this kind for any coronavirus. As kinases are key regulators of many cellular processes, the pro- and antiviral factors identified by this strategy should pinpoint cellular pathways that are important for SARS-CoV replication.

For SARS-CoV, screening of the kinome-directed library of 779 siRNA SMARTpools resulted in the identification of 90 antiviral and 40 proviral proteins. Canonical cellular processes and pathways in which these factors were strongly represented included inositol phosphate metabolism, signaling by Rho family GTPases, and SAPK/JNK signaling (Fig. 6). Many hits could also be mapped to the interleukin (IL)-2, -6, -8, and IL-17 signaling pathways, which have previously been implicated in controlling coronavirus infection and coronavirus-induced inflammation (reviewed in [65]). For example, the SARS-CoV spike (S) protein was shown to induce the expression of the pro-inflammatory cytokine IL-8 [360], and IL-6 and IL-8 levels were elevated in the serum of SARS-CoV-infected patients [360, 361]. Furthermore, mouse hepatitis virus (MHV) and infectious bronchitis virus (IBV) infections were reported to upregulate the synthesis of these same cytokines [362, 363]. Although our siRNA library screen did not target interleukins directly, the identification of (kinase-regulated) interleukin signaling pathways is in line with these earlier studies, and emphasizes their importance in SARS-CoV infection.

Coronavirus replication is associated with a cytoplasmic RVN of modified ER, including double-membrane vesicles and convoluted membranes [30]. Despite the in-depth characterization of their ultrastructure, the biogenesis of these membrane structures and the cellular factors involved have remained largely uncharacterized. For example, the membrane source of these virus-induced structures is still controversial, with advanced EM analyses showing the RVN to be derived from and continuous with the ER [30, 208, 295] and other studies implicating the autophagy pathway [54] or EDEMosomes [55] as the primary membrane source. Our earlier work already suggested that the integrity of the early secretory pathway is important for efficient SARS-CoV replication, as brefeldin A (BFA) treatment of SARS-CoV-infected cells significantly reduced replication as well as the accumulation of virus-induced membrane structures [295]. In line with these find-

ings, COPI-coated vesicles were also implicated in the biogenesis of MHV replication structures [364, 365]. In addition, SARS-CoV nsp3 was shown to interact with three COPI subunits [366]. In none of these previous SARS-CoV and MHV studies a complete block of virus replication could be achieved, neither by reducing COPI vesicle formation by depletion of one of the coatomer subunits, nor by treatment with BFA. These results might partially be explained by incomplete knockdown or the presence of residual COPI vesicles (complete knockdown is probably not possible due to its detrimental effect on intracellular trafficking and cell viability). Although our study clearly demonstrates the importance of COPI-vesicles in SARS-CoV replication, the role of COPI vesicles in the formation of the SARS-CoV-induced RVN remains elusive and requires a more in-depth

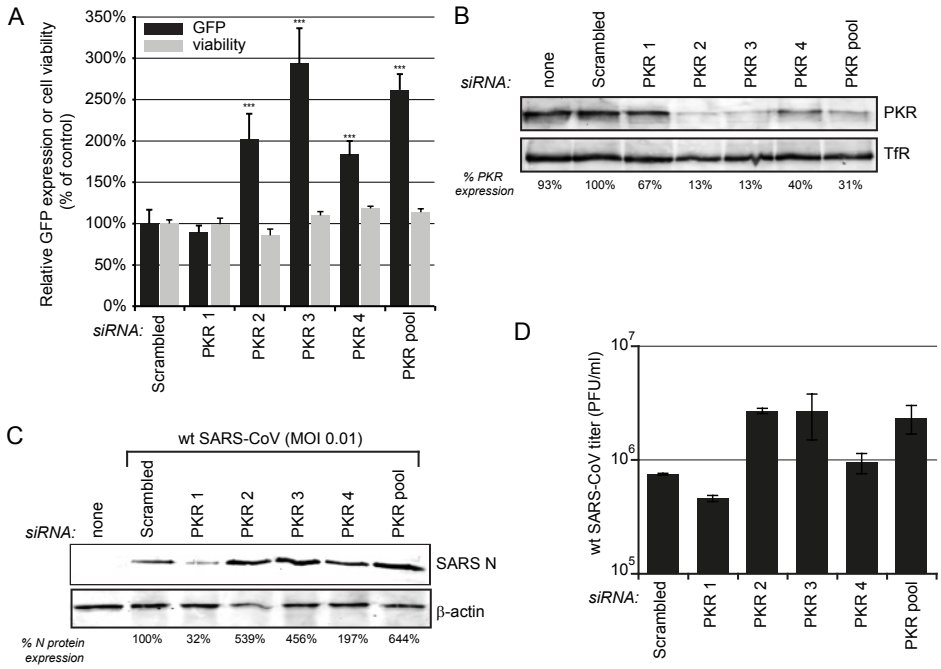

Fig. 8. Validation of PKR as an antagonist of SARS-CoV replication. 293/ACE2 cells were transfected with four individual siRNAs targeting PKR or a scrambled control siRNA. (A) At 48 h p.t. cells were infected with SARS-CoV-GFP (MOI 10), fixed 24 later, and GFP fluorescence (black bars) was quantified and normalized to the value measured in infected, scrambled siRNA-transfected cells (100%). The effect of siRNA transfection on cell viability was analyzed in parallel (grey bars) and values were normalized to those of scrambled siRNA-transfected control cells (100%). Average ± SD is given (***; p-value < 0.001). (B) Knockdown of PKR expression at 48 h p.t. was monitored by Western blotting with a PKR-specific antiserum and TfR was used as loading control. The percentage of remaining PKR expression compared to scrambled siRNA-transfected cells is shown below each lane. (C) Cells transfected with PKR specific siRNAs and control cells were infected with SARS-CoV (MOI 0.01) and 24 h later these cells were lysed to assess SARS-CoV N levels by Western blotting (shown below the panels as percentage of control), using β-actin as loading control. (D) Virus titers in the 24-h p.i. culture supernatants of wt SARS-CoV-infected cells (MOI 0.01) transfected with PKR-specific or scrambled siRNA.

analysis. The importance of COPI-coated vesicles is further supported by their essential role in the replication of many other RNA viruses, such as poliovirus [367, 368], other enterovirus family members [353, 369-371], vesicular stomatitis virus [372], Drosophila C virus [373], and influenza A virus [344, 374].

Interestingly, our screen yielded a relatively high proportion of antiviral hits, with PKR knockdown having one of the strongest effects (~2-fold increase of GFP expression in SARS-CoV-GFP-infected cells). During hit validation, three out of four individual PKR-directed siRNAs caused a clear increase in SARS-CoV protein expression and virus yield (Fig. 8C-D). PKR is one of four mammalian kinases that can phosphorylate eIF-2α in response to stress signals (the others being the PKR-like endoplasmic reticulum kinase (PERK), GCN2, and HRI). Many virus families have evolved gene products and strategies to counteract or evade the antiviral action of PKR, illustrating the importance of this kinase in the antiviral defense. Previously, it was found that PKR inhibits the replication of the coronavirus IBV, as overexpression of a kinase-defective PKR mutant enhanced IBV replication by almost 2-fold . Furthermore IBV appeared to (weakly) antagonize the antiviral activity of PKR through two independent mechanisms, including the partial blockage of PKR activation [69]. For the distantly related arterivirus porcine reproductive and respiratory syndrome virus (PRRSV), it was shown that IFN-β- [375] and IFN-γ-treated [376] MARC-145 cells were no longer permissive to infection, while treatment with the PKR inhibitor 2-aminopurine restored PRRSV replication. This suggests an important antiviral role for PKR in controlling PRRSV infection. Krähling *et al*. show that PKR was activated in SARS-CoV-infected 293/ACE2 cells, but conclude that knockdown of PKR did not significantly affect virus replication, despite the fact that a ~1-log increase in SARS-CoV titer was observed in their experiments [377]. This is in contrast to our PKR knockdown experiments that point to an antiviral role for PKR (Fig. 8). Our data clearly shows that depletion of PKR significantly increased SARS-CoV-driven GFP expression (Fig. 8A), and also enhanced N protein expression (Fig. 8C) and virus progeny release (Fig. 8D). This discrepancy cannot be due to host cell differences, as the same 293/ACE2 cells were used in both studies [377], and might be due to differences in the experimental set-up, choice of controls, or normalization and interpretation of data.

In line with the findings for PKR, reducing the expression of PERK (or EIF2AK3), one of the other kinases known to phosphorylate eIF-2α, resulted in an increase of SARS-CoV-GFP reporter gene expression by 57% ($p < 0.01$; Fig. 5A). The unfolded protein response - i.e. the detection of misfolded proteins within the ER lumen - activates PERK, which in turn phosphorylates eIF2α, and ultimately triggers apoptosis. The relatively strong antiviral effect of PERK observed in this study is in line with previous studies suggesting that the phosphorylation of eIF-2α in SARS-CoV-infected cells is mediated by the activation of PERK [377]. Our findings support the hypothesis that upon SARS-CoV infection the unfolded protein response is activated as an antiviral strategy. Multiple cellular re-

sponses that induce apoptosis, including the activation of PKR and PERK, might actually be involved in controlling SARS-CoV infection, which could also explain several other hits involved in apoptosis, like those from the SAPK/JNK pathway.

In conclusion, our kinome-wide siRNA screen has identified several cellular proteins and processes that influence SARS-CoV replication. These include novel factors that may play a role in coronavirus infections in general. Our data thus provide a starting point for further validation and in-depth mechanistic studies, preferably involving multiple factors from the identified pathways, which should enhance our understanding of the complex interplay between coronaviruses and their host.

ACKNOWLEDGMENTS

We thank Ali Tas, Emmely Treffers, and Maarten van Dinther for helpful discussions and excellent technical assistance and Shinji Makino for providing 293/ACE2 cells. We are grateful to Martijn Rabelink and Rob Hoeben (Department of Molecular Cell Biology) for sharing their lentivirus expertise and for providing plasmids and reagents for generating shRNA-expressing lentiviruses. This research was supported by TOP grant 700.57.301 from the Council for Chemical Sciences of the Netherlands Organization for Scientific Research (NWO-CW).